Quantitative FLIM-FRET Microscopy to Monitor Nanoscale Chromatin Compaction In Vivo Reveals Structural Roles of Condensin Complexes

Llères, David; Bailly, Aymeric P.; Perrin, Aurélien; Norman, David G.; Xirodimas, Dimitris P.; Feil, Robert

Published in:
Cell Reports

DOI:
10.1016/j.celrep.2017.01.043

Publication date:
2017

Document Version
Publisher's PDF, also known as Version of record

Cell Reports

Resource

Quantitative FLIM-FRET Microscopy to Monitor Nanoscale Chromatin Compaction In Vivo Reveals Structural Roles of Condensin Complexes

Graphical Abstract

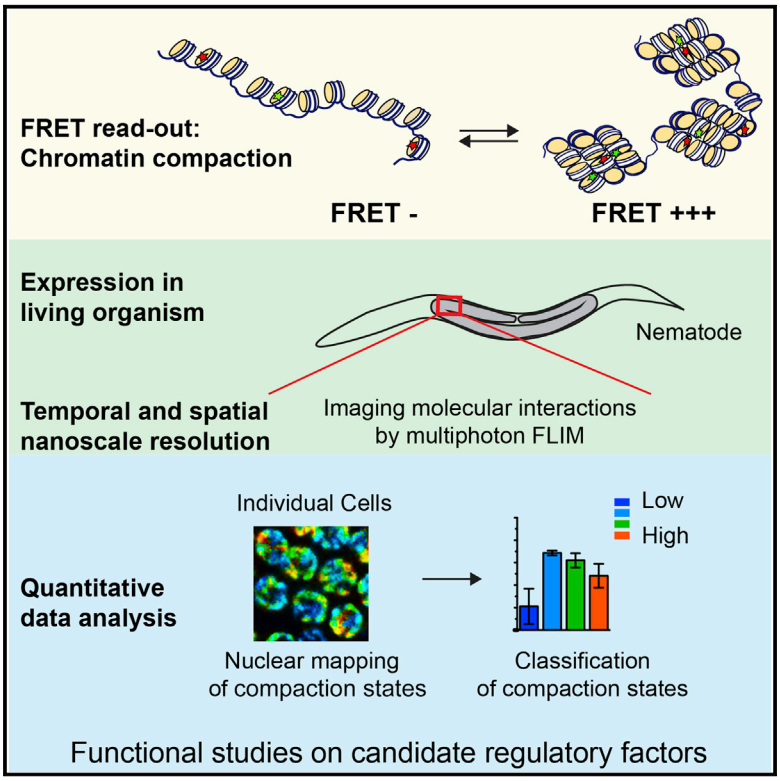

Highlights

- Meiotic chromosomes in living *C. elegans* display heterogeneous nanoscale compaction
- Heterochromatin has a compacted nanoscale organization controlled by HP1 and SETDB1 homologs
- Tandem repeat-enriched ectopic chromosomes acquire heterochromatic structure in meiotic cells
- Condensin I and II play essential roles in meiotic heterochromatin compaction

Authors

David Llères, Aymeric P. Bailly, Aurélien Perrin, David G. Norman, Dimitris P. Xirodimas, Robert Feil

Correspondence

david.lleres@igmm.cnrs.fr (D.L.), aymeric.bailly@crbm.cnrs.fr (A.P.B.), robert.feil@igmm.cnrs.fr (R.F.)

In Brief

How chromatin is structured in cells of living organisms remains poorly understood. Llères et al. adapted a FRET-based microscopic approach to monitor nanoscale chromatin compaction in the germline of living *C. elegans*. The study indicates heterogeneous compaction levels along pachytene chromosomes and reveals key roles of HP1 and condensin complexes.

Llères et al., 2017, Cell Reports *18*, 1791–1803
February 14, 2017
http://dx.doi.org/10.1016/j.celrep.2017.01.043

CellPress

Cell Reports
Resource

Quantitative FLIM-FRET Microscopy to Monitor Nanoscale Chromatin Compaction In Vivo Reveals Structural Roles of Condensin Complexes

David Llères,[1,2,5,6,*] Aymeric P. Bailly,[2,3,5,*] Aurélien Perrin,[2,3] David G. Norman,[4] Dimitris P. Xirodimas,[2,3] and Robert Feil[1,2,*]
[1]Institute of Molecular Genetics (IGMM), CNRS, UMR-5535, 34293 Montpellier, France
[2]University of Montpellier, 34090 Montpellier, France
[3]Cell Biology Research Center of Montpellier, CNRS, UMR-5237, 34293 Montpellier, France
[4]Nucleic Acids Structure Research Group, University of Dundee, Dundee DD1 5EH, UK
[5]Co-first author
[6]Lead Contact
*Correspondence: david.lleres@igmm.cnrs.fr (D.L.), aymeric.bailly@crbm.cnrs.fr (A.P.B.), robert.feil@igmm.cnrs.fr (R.F.)
http://dx.doi.org/10.1016/j.celrep.2017.01.043

SUMMARY

How metazoan genomes are structured at the nanoscale in living cells and tissues remains unknown. Here, we adapted a quantitative FRET (Förster resonance energy transfer)-based fluorescence lifetime imaging microscopy (FLIM) approach to assay nanoscale chromatin compaction in living organisms. *Caenorhabditis elegans* was chosen as a model system. By measuring FRET between histone-tagged fluorescent proteins, we visualized distinct chromosomal regions and quantified the different levels of nanoscale compaction in meiotic cells. Using RNAi and repetitive extrachromosomal array approaches, we defined the heterochromatin state and showed that its architecture presents a nanoscale-compacted organization controlled by Heterochromatin Protein-1 (HP1) and SETDB1 H3-lysine-9 methyltransferase homologs in vivo. Next, we functionally explored condensin complexes. We found that condensin I and condensin II are essential for heterochromatin compaction and that condensin I additionally controls lowly compacted regions. Our data show that, in living animals, nanoscale chromatin compaction is controlled not only by histone modifiers and readers but also by condensin complexes.

INTRODUCTION

The eukaryotic genome is packaged into chromatin composed of a basic, repetitive unit called a nucleosome (Luger et al., 1997). Regularly spaced nucleosome arrays have been shown to fold into organized structures, which can be condensed into different secondary and tertiary higher order chromatin configurations (Luger and Hansen, 2005; Woodcock and Dimitrov, 2001). Many nuclear events and genome functions have been linked to the heterogeneous structuration of chromatin in metazoans (Bickmore, 2013; Cremer et al., 2004; Gibcus and Dekker, 2013). Furthermore, proper development of organisms depends on the regulation of gene activity, which involves the packaging of the genome into transcriptionally active and inactive chromatin domains (Jenuwein and Allis, 2001; Sexton et al., 2007). Despite the emergence of novel technologies, it remains a challenge to understand how chromatin is structured and packaged at the nanoscale in individual cells of living organisms (Boettiger et al., 2016; Lieberman-Aiden et al., 2009; Linhoff et al., 2015).

Chromosome architecture and levels of compaction have been widely explored by using DNA fluorescence in situ hybridization (FISH) and chromosome conformation capture (3C) techniques (Cremer et al., 2008; Dixon et al., 2012; Lieberman-Aiden et al., 2009). More recently, ex vivo super-resolution imaging by 3D stochastic optical reconstruction microscopy (STORM) was applied and, combined with DNA FISH with fluorescently labeled oligonucleotides, has demonstrated that epigenetically defined sub-megabase domains have distinct folding characteristics in *Drosophila* nuclei (Boettiger et al., 2016). Although the current microscopic and 3C-based technological approaches are powerful and generate a spatial resolution of $\leq$50 nm and high-resolution interaction maps, they are performed on populations of cells and involve cross-linked chromatin, cell fixation, or the use of probes limited to a small number of genetic loci. Conversely, analysis of chromatin in intact living cells has been hampered by limitations in the diffraction-limited resolution of light microscopy that gathers information at spatial scales larger than ~200–300 nm, so that structural chromatin folding at the nanoscale can be missed (Maddox et al., 2006; Mora-Bermúdez and Ellenberg, 2007; Strukov and Belmont, 2009). Therefore, currently available methodologies provide only indirect and limited information about the regulation of the nanometer scale configuration of chromatin in the cells of living organisms, in which there is a complex relationship between chromatin organization, gene regulation and the environment.

Overcoming the technical difficulties for determining nanoscale chromatin compaction, we developed a non-invasive methodology that allows one to map and quantify levels of

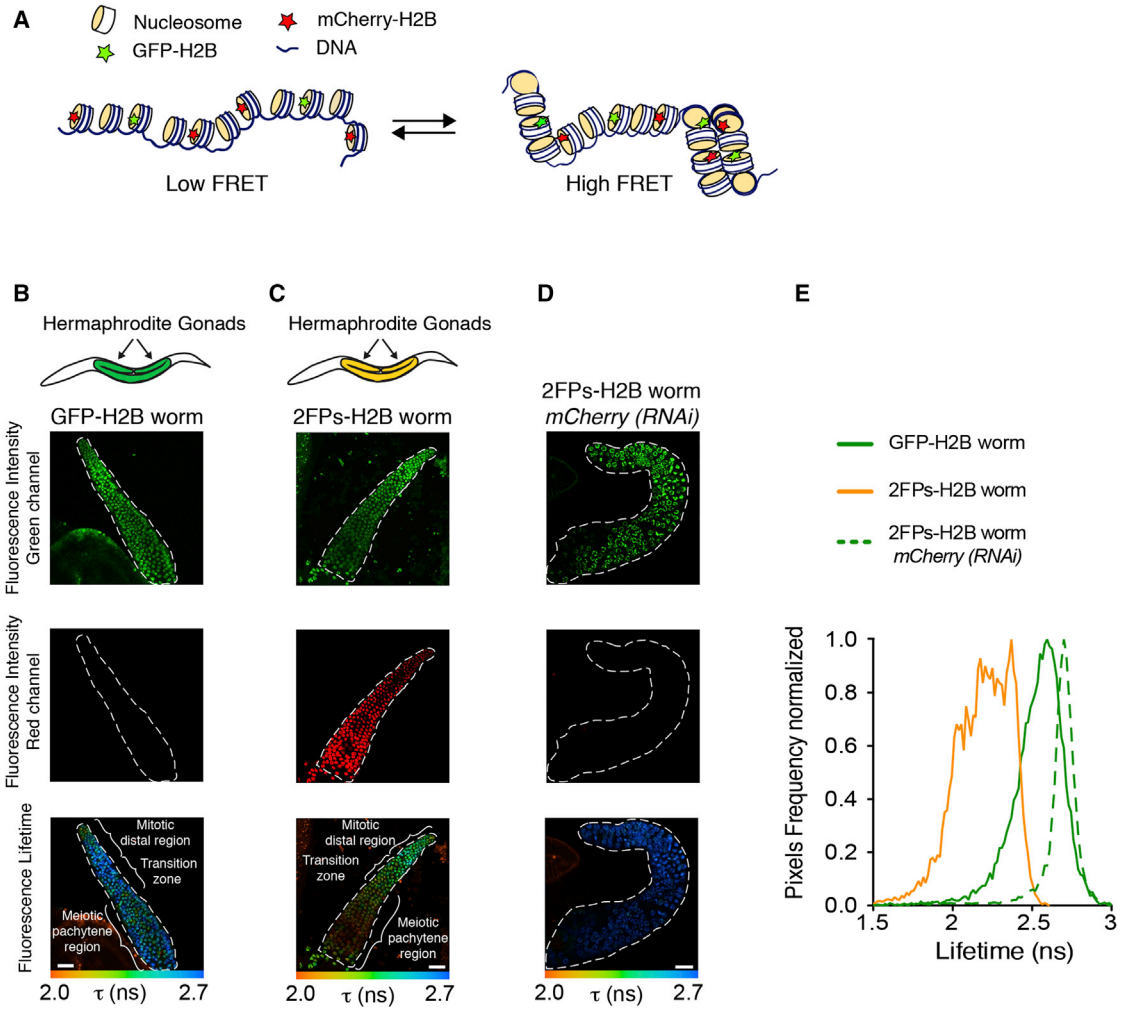

Figure 1. Chromatin Compaction Monitored by FLIM-FRET in Gonads of Living Adult *C. elegans*

(A) Schematic presentation of how tagged-histone FLIM-FRET monitors nanoscale chromatin compaction; the shown example structures are theoretical.

(B) Gonads from *C. elegans*$^{GFP::H2B}$ worms (named GFP-H2B) were imaged using multiphoton laser scanning microscopy. Fluorescence intensities in the green (upper panel) and red (middle panel) channels are shown. The mean fluorescence lifetime (τ) was determined for each pixel (lower panel). Its spatial variation is shown, with τ values represented by a pseudo-color scale ranging from 2.0 to 2.7 ns.

(C) Gonads from *C. elegans*$^{GFP::H2B/mCherry::H2B}$ worms (named 2FPs-H2B) were imaged, and the GFP and mCherry fluorescence intensities are shown. The spatial distribution of the mean τ (ns) is depicted.

(D) Representative gonad from a 2FPs-H2B worm after *mCherry(RNAi)* depletion.

(E) Mean τ value distribution curves in gonads of GFP-H2B (donor), 2FPs-H2B (donor/acceptor), and 2FPs-H2B *mCherry(RNAi)*-depleted (acceptor-depleted) worms are shown.

Scale bars, 20 μm.

See also Figures S1 and S2.

chromatin compaction (Figure 1A). In brief, our assay is based on fluorescence lifetime imaging microscopy (FLIM) to measure Förster resonance energy transfer (FRET) between histone-tagged fluorescent protein fusions. The FLIM approach has the advantage of measuring the fluorophore lifetime of the donor protein species only. It provides accurate quantification due to the independence of the fluorescence lifetime from the relative concentrations of the interacting proteins and is independent of its diffusion rates. Based on this underlying idea, we previously reported a FRET-based methodology in which we assayed energy transfer between fluorescently tagged core histones incorporated into the chromatin of HeLa cancer cells (Llères et al., 2009). The extent of FRET and its spatial distribution within nuclei were quantified by FLIM. Since FRET occurs only when a donor- and an acceptor-tagged histone are positioned less than 10 nm apart, this combined FLIM-FRET approach yielded a spatial readout of nanoscale chromatin compaction in the nuclei of the studied HeLa cells (Llères et al., 2009).

We decided to make use of two-photon FLIM measurements, which have the advantage of minimizing the effect of photon

scattering in thick layers of sample. Being, therefore, less affected by the heterogeneous nature of living tissues, we explored whether quantitative multiphoton FLIM-FRET on tagged H2B histones (Figure 1A) can be adapted to a living organism. We chose *C. elegans* as a model system. Their transparency makes these worms highly suitable for fluorescence microscopy imaging. *C. elegans* allows also efficient gene knockdown by RNAi, an advantage that we exploited to explore the in vivo roles of candidate regulators of chromatin compaction in the germline.

Using the FLIM-FRET assay adapted to living *C. elegans*, we spatially reveal distinct domains and quantitatively discriminate different levels of chromatin compaction in pachytene meiotic germ cells. By using RNAi and exogenous extra-chromosomal repeat arrays, we uncover the structural architecture of heterochromatin. We show that its high degree of nanoscale compaction is regulated by Heterochromatin Protein-1 (HP1) and SETDB1 H3-lysine-9 methyltransferase homologs and that its formation is linked to the presence of repeated sequence elements. Furthermore, we investigate whether regulators of higher order features of chromosomes have an impact on the nanoscale packaging of chromatin as well. We found that, in pachytene-stage germ cells, depletion of the condensin I subunit DPY-28 affects heterochromatin and also lowly compacted regions, whereas the condensin II subunit KLE-2 is required for heterochromatin compaction only. Our combined experimental data establish that the differential nanoscale compaction of chromatin in vivo depends not only on epigenome writers and readers but also on different condensin complexes. The latter finding implies that the three-dimensional chromosome architecture controlled by condensins is functionally linked to the nanoscale compaction of chromatin. This emerging biological insight should help to better understand gene regulation and developmental processes such as meiosis.

RESULTS

For this in vivo FLIM-FRET study, we investigated chromosome and chromatin dynamics in the germline, the best characterized *C. elegans* lineage for chromatin (Bessler et al., 2010; Mets and Meyer, 2009). We exploited strains that stably expressed either GFP-H2B alone (a strain hereinafter called "GFP-H2B") or both the GFP-H2B and mCherry-H2B fusion proteins (FPs) (strain "2FPs-H2B") from a single transcription unit driven by the germline-specific *pmex-5* promoter to achieve endogenous expression levels in the germline (Frøkjær-Jensen et al., 2012) (Figures S1A and S1B). Immunoblotting of chromatin-enriched protein fractions showed that the H2B fusion proteins were expressed appropriately and migrated at the expected sizes and represented about 4% of total histone H2B (Figure S1C). Compared to the wild-type N2-Bristol strain, early mitotic divisions were normal in the 2FPs-H2B embryos (Figure S1D). Development and fertility were also unaffected in the two transgenic lines, which suggested that the expression of GFP-H2B and mCherry-H2B had not interfered with vital functions (Figure S1E). As expected, the GFP-H2B and mCherry-H2B histones co-localized within the nucleus, and their distribution overlapped with that of genomic DNA, indicative of homogeneous incorporation into chromatin (Figure S1F). Fluorescence recovery after photobleaching (FRAP) analysis of strains GFP-H2B and 2FPs-H2B showed a slow recovery of the tagged histones after photobleaching, consistent with their stable incorporation into chromatin (Figure S1G).

Nanoscale Chromatin Compaction Monitored by FLIM-FRET in Living *C. elegans*

Gonads from adult hermaphrodites were imaged following two-photon excitation at 890 nm. The mean fluorescence lifetime (i.e., time spent in the excited state) (τ, in nanoseconds) of GFP-H2B donor proteins was measured by FLIM in each pixel. When FRET occurs, at a range of 1–10 nm, the donor's (GFP-H2B) lifetime is reduced due to energy transfer to the acceptor fluorophore (mCherry-H2B). A marked decrease of the GFP-H2B τ value (τ = 2.3 ns) was detected in 2FPs-H2B gonads compared to GFP-H2B gonads (τ = 2.6 ns) (Figures 1B, 1C, and 1E). The GFP-H2B τ reduction was no longer observed after RNAi-mediated depletion of mCherry-H2B (τ = 2.7 ns), which confirms that the marked effect was due to FRET (Figures 1D and 1E; Figure S2A). To rule out possible confounding effects due to FRET between GFP-H2B and mCherry-H2B proteins incorporated into the same nucleosome, we performed molecular modeling based on the known nucleosome structure (Luger et al., 1997). This showed that the distance separating the GFP and mCherry attachment sites, on the two H2B histones, was too large (130 Å on average) to produce significant intra-nucleosomal FRET (Figure S2B). Combined, these data demonstrate our ability to monitor fluorescence lifetime by multiphoton FLIM in living animals and that FRET occurs from interactions between fluorescent-tagged H2B histones incorporated in different, but spatially close, nucleosomes as a result of chromatin compaction.

Spatial Organization of Chromatin Compaction Levels in Pachytene Cells

Like in mammals, when reaching the pachytene stage of germ cell development, *C. elegans* chromosomes have acquired a highly ordered structuration that is essential for subsequent crossing over, recombination, and chromosome segregation to occur (Lui and Colaiácovo, 2013). Accordingly, we observed the strongest reduction of GFP-H2B τ within the meiotic pachytene region of the gonads in 2FPs-H2B worms (Figures 1C and S3A). Indeed, quantification of GFP-H2B τ in the cells at the pachytene stage showed a significant decrease of the mean lifetime τ (τ = 2.39 ± 0.09 ns, relative to τ = 2.64 ± 0.06 ns in GFP-H2B worms) (Figures 2A and 2B; Table S1). FRAP experiments established that this lifetime decrease was not due to an altered rate of tagged-histone exchange (Figure S1G). Since pachytene chromosomes are highly structured, we verified that the marked reduction in GFP-H2B τ was not caused by local concentration of the GFP-H2B donor alone. Importantly, no obvious correlation (r = 0.22) was detected between the measured GFP-H2B τ and the corresponding GFP-H2B photon counts (Figure S3B). Quantification and spatial mapping of FRET in the individual nucleus of 2FPs-H2B pachytene-stage cells revealed discrete regions in the nucleus associated with

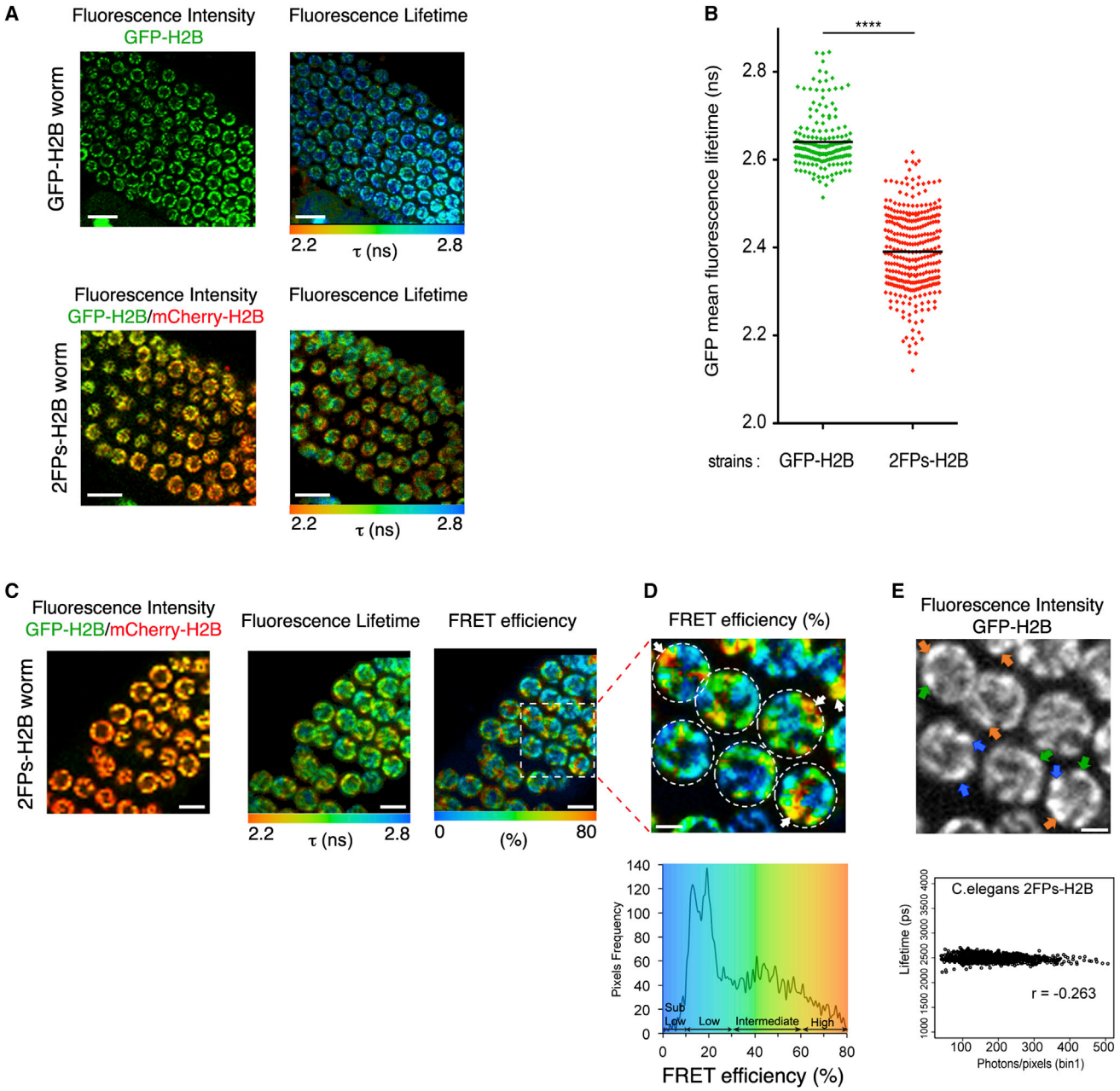

Figure 2. Spatial Organization of Chromatin Compaction Levels in Pachytene Cell Nuclei

(A) Higher magnifications of confocal (left) and FLIM (right) images of GFP-H2B and 2FPs-H2B pachytene-stage cells. Fluorescence lifetime (τ) values are presented in a continuous pseudo-color scale ranging from 2.0 to 2.8 ns. Scale bar, 10 μm.

(B) Scatterplots show the mean GFP fluorescence lifetime distribution in GFP-H2B (green diamonds; 195 cells, n = 7 gonads) and 2FPs-H2B (red diamonds; 327 cells, n = 10 gonads) worms. GFP lifetime is significantly reduced in 2FPs-H2B gonads compared to GFP-H2B gonads. ****$p < 0.0001$ (two-tailed Mann-Whitney test); 95% confidence interval.

(C) Fluorescence intensity (left), FLIM (middle), and FRET (right) images of 2FPs-H2B cells. The spatial variation in the FRET efficiency is depicted (color scale ranges from 0% to 80%). Scale bars, 5 μm.

(D) Upper panel: higher magnification of nuclei (from C) reveals regions with distinct FRET efficiencies. White arrows highlight specific high-FRET regions. Meiotic nuclei are outlined with dashed lines. Scale bar, 2 μm. Lower panel: FRET efficiency variation graph showing distinct populations. Low (in blue), FRET efficiency between 10% and 30%; intermediate (in green), FRET efficiency between 30% and 60%; and high (in orange), FRET efficiency between 60% and 80%.

(E) Upper panel: high densities of GFP-H2B histone do not correlate with high-FRET percent regions. The orange, green, and blue arrows indicate example regions with high-, intermediate-, and low-FRET percent regions, respectively, that are all of high GFP-H2B density. Lower panel: plot of GFP-H2B fluorescence lifetime versus GFP photon count in the 2FPs-H2B strain. The calculated Pearson r correlation coefficient is indicated. Scale bar, 2 μm.

See also Figure S3 and Table S1.

distinct FRET efficiencies (Figures 2C and 2D). These were arbitrarily grouped into four different classes: "sub-low FRET" (FRET efficiencies between 0% and 10%; dark blue), "low FRET" (efficiencies between 10% and 30%; light blue), "intermediate FRET" (efficiencies between 30% and 60%; green) and "high FRET" (efficiencies between 60% and 80%; orange) (Figures 2D and S3C). Single z sections included multiple distinct high-FRET regions across the nucleus and showed that these highly compacted regions were not confined to one pair of chromosomes. Specifically, in our in vivo acquisitions, we did not detect high FRET corresponding to a unique compact globular structure associated to the X chromosome, as observed after immunocytochemistry experiments in *C. elegans* (Kelly et al., 2002). Although pachytene-stage chromosomes are highly structured throughout, we find that their nanoscale compaction is highly uneven along the chromosomes. Some regions are highly compacted, whereas others comprise lowly compacted chromatin. Interestingly, by comparing the fluorescence intensity of GFP-H2B reflecting the nucleosome density along DNA with the FRET efficiency map (Figures 2E and 2D, respectively), we ascertained that the bright nucleosome-dense regions (Figure 2E, colored arrowheads) were not exclusively associated to high-FRET regions (orange arrowheads) but also corresponded to intermediate (green arrowheads) and low-FRET (blue arrowheads) regions. This general observation was confirmed by finding a negative linear relationship ($r = -0.263$) between GFP-H2B intensity and GFP-H2B lifetime in 2FPs-H2B cells (Figure 2E, graph). This key finding indicates that FRET pixels are not simply reflecting clustered regions of chromatin but, rather, reflect the local packing state of chromatin.

The HP1 Homolog HPL-2 Is Essential for Heterochromatin Compaction

To evaluate whether the tagged-histone FRET assay monitors chromatin compaction levels associated to a defined epigenetic status of chromatin, we studied repressed chromatin that is marked by histone H3 lysine 9 methylation and bound by heterochromatin protein-1 proteins. Even though HP1 mediates silent chromatin (Danzer and Wallrath, 2004; Wallrath and Elgin, 1995), its contribution to in vivo nanoscale chromatin compaction has not been determined. Similarly, as in mammals (Richards and Elgin, 2002), HPL-2 (the main HP1 homolog in *C. elegans*) and H3-lysine-9 dimethylation (H3K9me2) define heterochromatin in *C. elegans*, which, in this species, is largely confined to the distal and proximal parts of the autosomes (Couteau et al., 2002; Garrigues et al., 2015) (Figure S4A, top row). Upon RNAi against *hpl-2*, the comparative FLIM-FRET analysis of 2FPs-H2B worms revealed a significant decompaction, as indicated by a longer GFP-H2B τ and a concomitantly reduced FRET efficiency (Figures 3A and 3B). We confirmed that there was no developmental delay, since this could have explained, in part, the observed chromatin decompaction (Figure S4B). Importantly, *hpl-2(RNAi)* strongly reduced the high- and intermediate-FRET populations, without affecting the low-FRET population (Figure 3C; Figure S4C). Our findings indicate that heterochromatin is organized into a nanoscale-compacted architecture in vivo and that HPL-2 plays an essential role in this nanometer scale compaction.

MET-2 Histone Methyltransferase Controls Heterochromatin Compaction

The role of H3K9me2 in repressive chromatin compaction was assessed by RNAi against *met-2*, the *C. elegans* homolog of lysine methyltransferase *SETDB1* (Andersen and Horvitz, 2007; Bessler et al., 2010) (Figure 4A). The resulting almost-complete loss of H3K9me2 correlated with an overall reduced compaction of chromatin (Figures 4B and 4C; Table S1), caused by loss of the "high" and "intermediate" chromatin populations (Figure 4D). In agreement with previous studies (Bessler et al., 2010; Garrigues et al., 2015), no alteration in the staining patterns of HPL-2 and H3K9me3 was detected in *met-2(RNAi)*-depleted cells (Figures S4A and S4D, respectively). These findings show that the methyltransferase MET-2 promotes heterochromatin compaction. Although HPL-2 staining seemed, globally, not altered in *met-2(RNAi)* pachytene cells, we cannot exclude that a minor fraction of HPL-2 bound to H3K9me2 is lost upon *met-2(RNAi)* and contributes to the decompaction detected by FLIM-FRET. The combined results indicate that HPL-2 and MET-2 are both important for nanoscale heterochromatin compaction and that their functions are not necessarily independent.

A consistent feature of heterochromatin, including in nematodes, is the repetitive nature of its associated DNA (Stinchcomb et al., 1985). In *C. elegans* germ cells, micro-injected exogenous DNA can induce gene silencing through the formation of tandemly repeated arrays (Kelly et al., 1997). Such extra-chromosomal concatemers display hallmarks of heterochromatin, including H3K9me2/3 enrichment (Kelly et al., 2002; Towbin et al., 2010). To determine whether ectopic repeated DNA sequences can bring about compacted chromatin, we injected the well-studied array-forming plasmid pRF4 (Kramer et al., 1990) into the gonads of 2FPs-H2B worms (Figure S5) and generated F1 offspring. A strong enrichment of HPL-2 and H3K9me2 was detected at the formed transgene arrays in the gonads of the F1 offspring (Figure 5A, arrowheads). Strikingly, high-FRET globular signals coincided with the extra-chromosomal arrays (Figure 5B, arrowheads). Concordantly, we measured an overall increase of high-FRET chromatin in the pRF4-containing F1 gonads (Figure 5C). The additional high-FRET signal due to the plasmid array disappeared following *hpl-2(RNAi)* depletion (Figure 5C). This finding highlights a similar role of HPL-2 at the exogenous transgene array as that at endogenous heterochromatin. The combined data evoke a general model in which repeated DNA elements induce compacted, heterochromatic structuration through the recruitment and actions of HPL-2 and MET-2.

Condensin Complexes Are Essential for the Nanoscale Compaction of Heterochromatin

Architectural proteins organize the genome at different length scales (Phillips-Cremins et al., 2013). We investigated whether the evolutionarily conserved condensin complexes, which regulate higher order chromosome configurations (Hirano, 2005), play a role in nanoscale chromatin compaction in vivo. In mouse oocytes, condensins are required for chromosome-thread formation and chromosomal rigidity, and immune-FISH studies

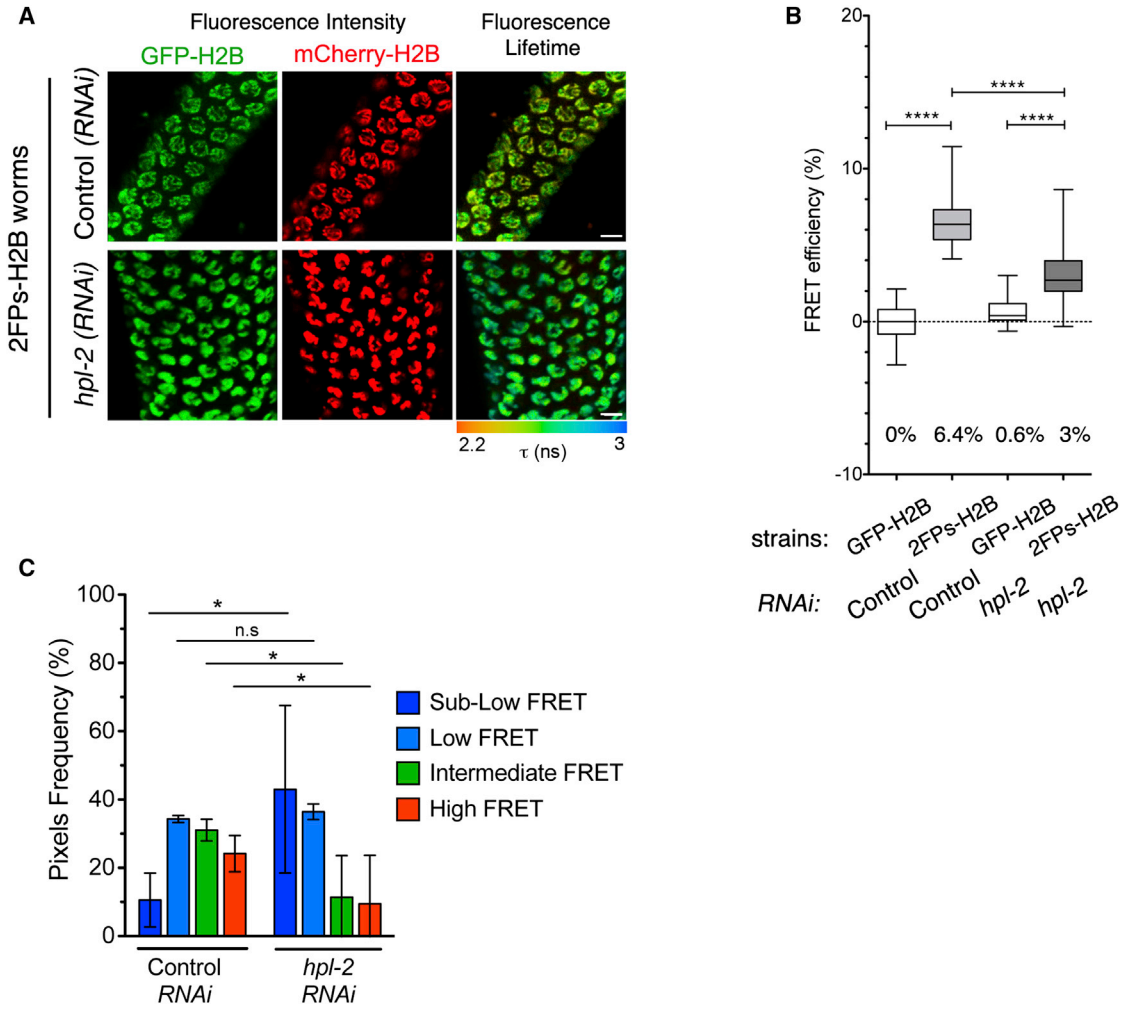

Figure 3. HP1 Homolog HPL-2 Controls the Nanometer Scale Compaction of Heterochromatin

(A) GFP-H2B and mCherry-H2B expression is unaffected by *hpl-2(RNAi)* depletion. Spatial distribution of the fluorescence lifetime in 2FPs-H2B pachytene cells following control (*RNAi)* and *hpl-2(RNAi)* depletion (bottom). Bars, 5 μm.

(B) Box-and-whisker plots show the FRET efficiency (percentage) for each condition; the mean FRET efficiency value is indicated at the bottom of each box. ****$p < 0.0001$, two-tailed Mann-Whitney test.

(C) The relative fraction of the four FRET populations—sub-low (FRET efficiency between 0% and 10%), low, intermediate, and high—in control *(RNAi)* and *hpl-2(RNAi)* (100–120 cells from three gonads per condition). *$p < 0.05$ (two-tailed unpaired t test); n.s, nonsignificant.

See also Figure S4 and Table S1.

have shown that disruption of condensins I and II extends meiotic chromosome axes in *C. elegans* (Houlard et al., 2015; Mets and Meyer, 2009). However, the structural basis of these effects and their consequences for nanoscale heterochromatin compaction are not known.

DPY-28 is an essential component both of condensin I and condensin I^{DC} complexes, which regulate meiotic crossover distribution and frequency in germ cells and X chromosome dosage compensation (DC) in somatic cells, respectively (Csankovszki et al., 2009; Mets and Meyer, 2009; Tsai et al., 2008). *dpy-28(RNAi)* depletion (Figure S6A) induced nanoscale decompaction of pachytene chromatin (Figure 6A; Figures S6B and S6C; Table S1). It affected heterochromatin mainly (high and intermediate), but also the less compacted chromatin (low) (Figure 6B). Similarly, as reported for fixed cells (Mets and Meyer, 2009), the essential condensin II subunit KLE-2 is involved in the regulation of meiotic chromatin compaction (Figure 6A; Figures S6B and S6C; Table S1). However, we found that condensin II controls heterochromatin only, and its depletion did not affect the less compacted chromatin (Figures 6A and 6B). Combined depletion of the two condensin complexes by *dpy-28;kle-2(RNAi)* led to globally unstructured chromosomes in gonads, with the disappearance of the heterochromatin and less-compacted chromatin populations, which resulted in a unique population of "sub-low" FRET (Figure 6A; Figures S6B and S6C; Table S1). Staining of HPL-2 in *dpy-28(RNAi)*- and *kle-2(RNAi)*-depleted gonads showed that condensin depletion did not markedly interfere with HPL-2 recruitment onto chromatin

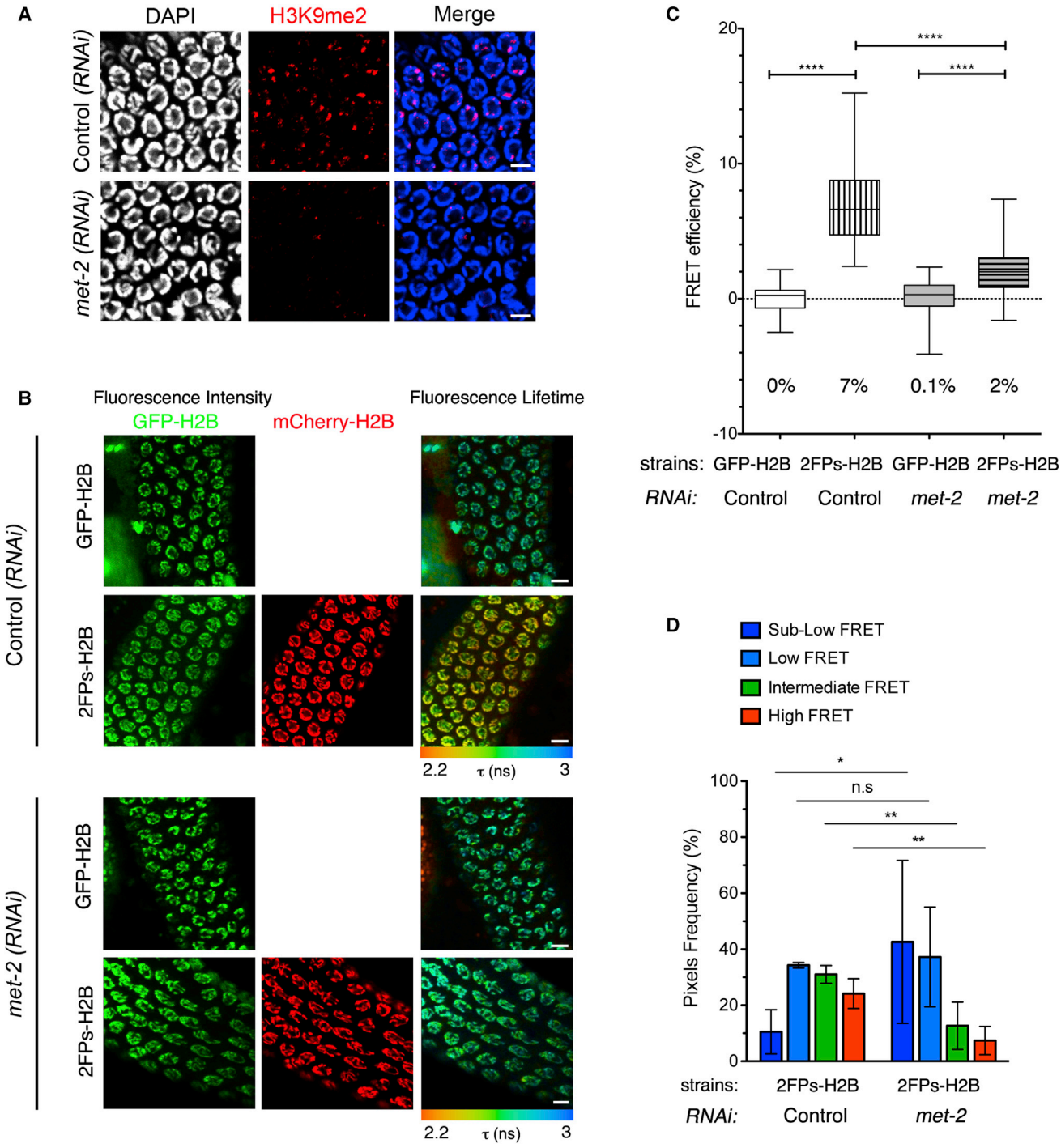

Figure 4. MET-2 Controls Heterochromatin Compaction

(A) Top: control *(RNAi)* pachytene germ cell nuclei. H3K9me2 (red) is concentrated in a subset of chromosomal regions. Bottom: in *met-2(RNAi)* pachytene nuclei, hardly any H3K9me2 is detected. Chromosomes were stained with DAPI (blue). Scale bars, 5 μm.

(B) The spatial distribution of fluorescence lifetime is shown for 2FPs-H2B cells from control *(RNAi)* (top panels) or *met-2(RNAi)* animals (bottom panels). Fluorescence lifetime values ranging from 2.2 ns to 3 ns are represented using a continuous pseudo-color scale. Scale bars, 5 μm.

(C) Statistical analysis of the FRET efficiency percentage for each condition, presented as box-and-whisker plots. The mean FRET efficiency value is indicated at the bottom of each box. ****$p < 0.0001$ (two-tailed Mann-Whitney test).

(D) The relative fraction of the four FRET populations (sub-low, low, intermediate, and high) in nuclei (100–120 cells from n = 3 gonads) from control *(RNAi)* and *met-2(RNAi)* cells. *$p < 0.05$; **$p < 0.01$ (two-tailed unpaired t test); n.s, nonsignificant.

See also Figure S4 and Table S1.

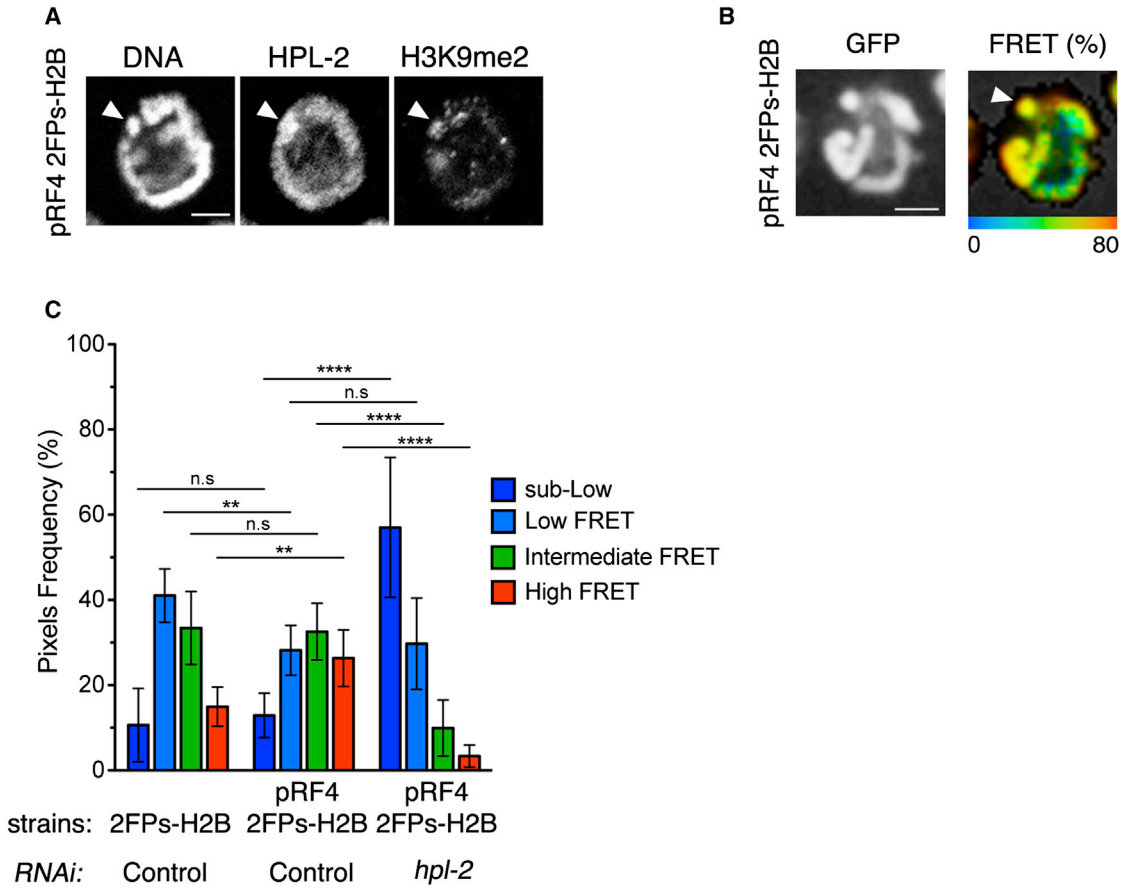

Figure 5. Tandem Repeat-Enriched Ectopic Chromosomes Acquire Heterochromatic Structure in Meiotic Cells

(A) In 2FPs-H2B gonads, the extra-chromosomal transgene array pRF4 is clearly visible as a distinct globule (arrowhead) in each nucleus, and its chromatin is enriched in HPL-2 and H3K9me2. Chromosomes are stained with DAPI. Scale bar, 2 μm.

(B) Chromatin at the pRF4 transgene array shows high FRET (arrowheads). Scale bar, 2 μm.

(C) Distribution of FRET populations in pRF4-injected 2FPs-H2B worms and following *hpl-2 RNAi* depletion. **p < 0.01; ****p < 0.0001 (two-tailed Mann-Whitney test); n.s, nonsignificant.

See also Figure S5.

(Figure S6D). Thus, condensins seem to contribute to heterochromatin compaction through a mechanism independent of HPL-2 recruitment.

To examine further the differential effects of condensin I or II on chromosome structure, we manually traced and plotted the FRET efficiencies profile along individual wild-type and *dpy-28*- or *kle-2(RNAi)*-depleted pachytene chromosomes. Wild-type chromosome showed high-FRET pixels alternating with intermediate-FRET pixels (Figure 6C). In contrast, we observed "high-intermediate" FRET alternating with "low to sub-low" FRET pixels in *dpy-28(RNAi)*-depleted chromosome, whereas *kle-2(RNAi)*-depleted chromosome displayed continuous low-FRET pixels with some remaining intermediate-FRET regions at the chromosome extremities (Figure 6C).

Combined, the aforementioned findings indicate that, besides their common roles, condensin I and condensin II complexes have specific functions in chromatin compaction, particularly in the context of the highly ordered lampbrush structure of meiotic chromosomes.

DISCUSSION

We developed an imaging methodology to monitor chromatin compaction in living animals and used it to explore the *C. elegans* germline. This in vivo assay defines chromatin compaction as nanoscale proximity between nucleosomes, measured through FRET between stably incorporated GFP-H2B and mCherry-H2B histones. We found that the structuration of chromosomes in developing germ cells involves a global increase in compaction. At the pachytene stage, the overall fluorescence lifetime had become substantially reduced because of extensive FRET occurring between the incorporated fluorescent histones. At this developmental stage, heterogeneously structured chromatin regions with different degrees of compaction are apparent along the chromosomes.

Additionally, our combined data define the largely autosomal heterochromatin in *C. elegans* (Garrigues et al., 2015) as a highly condensed structure in vivo and show that its nanoscale compaction is controlled by HPL-2 and MET-2 (Figure 7). In

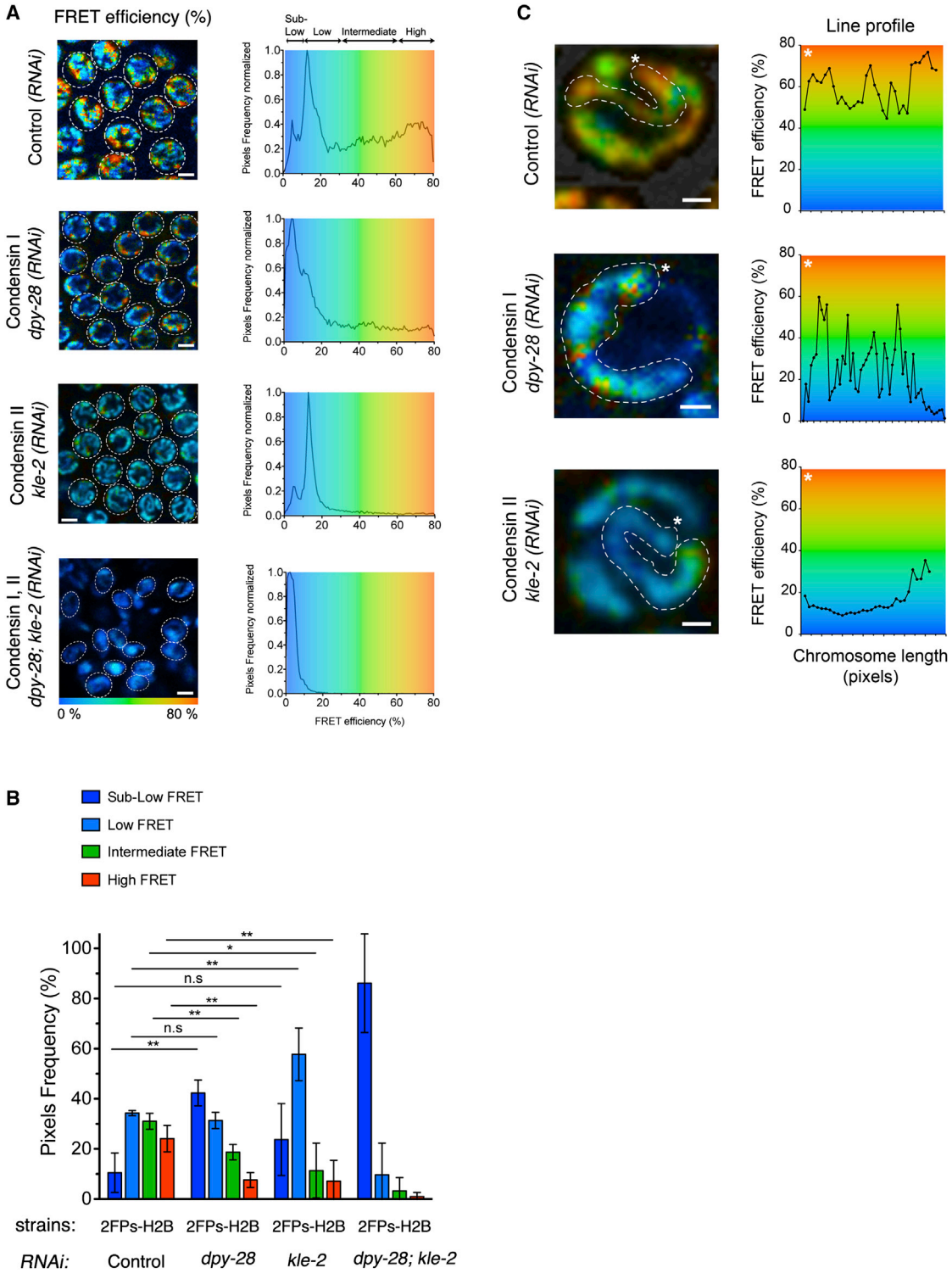

Figure 6. Condensin I and II Complexes Are Essential for Meiotic Heterochromatin Compaction

(A) Representative pachytene nuclei (left) and the spatial distribution of FRET regions (sub-low, low, intermediate, and high) (right) indicative of different chromatin compaction states after control *(RNAi)* and RNAi depletion of different condensin subunit genes (*dpy-28*, *kle-2*, and *dpy-28;kle-2*). Scale bars, 2 μm.

(B) Relative fraction of the four FRET populations (sub-low, low, intermediate, and high) in pachytene nuclei following control *(RNAi)* and *dpy-28(RNAi)*, *kle-2(RNAi)*, and *dpy-28;kle-2(RNAi)* (100–120 cells from three gonads per condition). *$p < 0.05$; **$p < 0.01$ (two-tailed unpaired t test); n.s, not significant.

(legend continued on next page)

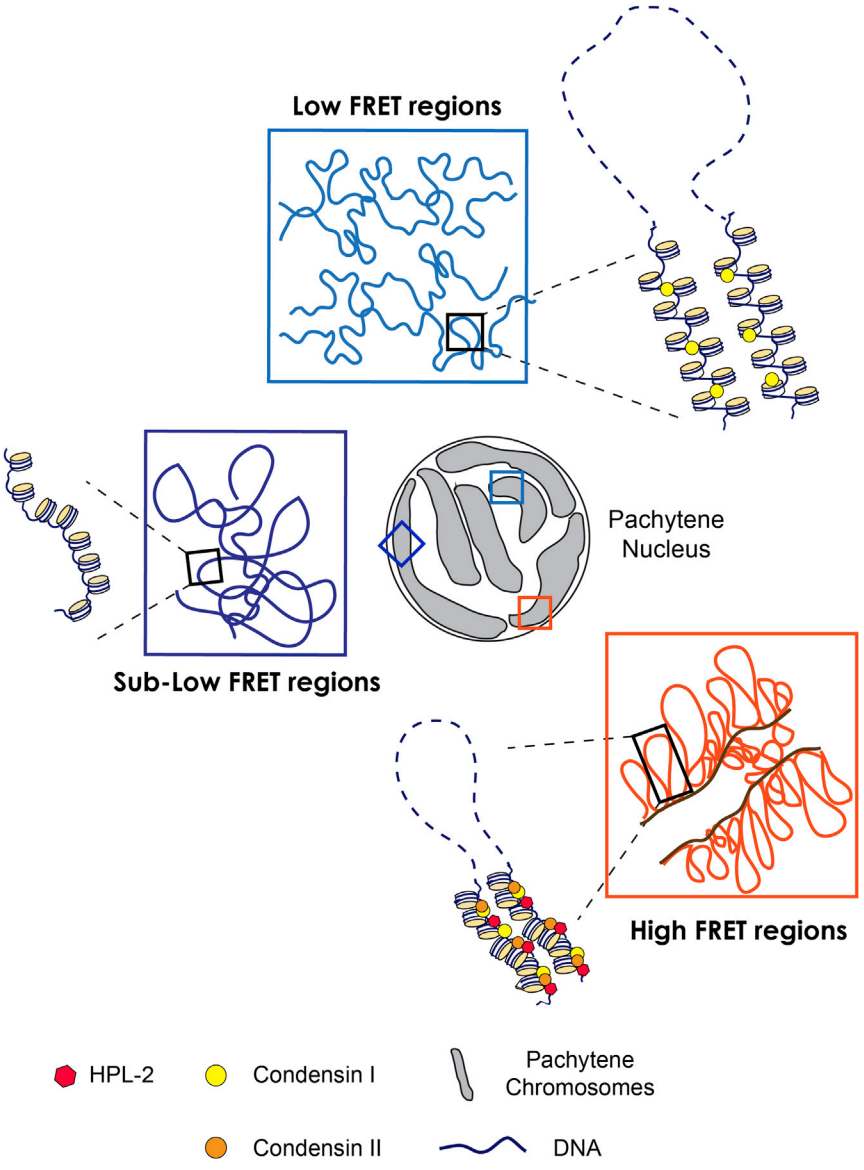

Figure 7. Summary Model for In Vivo Meiotic Chromatin Compaction

At the pachytene stage, meiotic chromosomes have acquired regions with different levels of nanoscale compaction (dark blue, light blue, and orange square boxes). Within the highly ordered lampbrush structure of meiotic chromosomes, heterochromatin compaction (high-FRET regions) is regulated by the HP1 homolog HPL-2 (red symbols) and by H3-lysine-9 methyltransferase MET-2, a homolog of SETDB1. Condensin complexes control local nanoscale compaction as well. Whereas condensin II (orange symbols) regulates heterochromatic chromatin predominantly, condensin I (yellow symbols) controls both heterochromatin and lowly compacted chromatin (low-FRET regions). At regions that show little or no FRET (sub-low-FRET regions), condensin complexes are presumed to be absent. The differential nanoscale compaction activities associated to condensin complexes may drive distinct morphological changes linked to loop array formation and to longitudinal chromosome axis rigidity, respectively. These may, in turn, affect the structural properties of chromosomes, such as the longitudinal rigidity of orthogonal axes, the number of chromatin loops, the position of loops, loop size, and, consequently, the meiotic recombination landscape.

met-2(RNAi) worms, the loss of H3K9me2 correlated with heterochromatin decompaction, although HPL-2 binding was not markedly reduced. This supports a recent study, which shows that HPL-2 can associate with chromatin in an H3K9me2-independent manner (Garrigues et al., 2015). Paradoxically, in hermaphrodite worms, the autosomal chromosome arms are enriched in HPL-2 but show higher recombination rates than central chromosomal regions, which do not show binding of HPL-2 (Barnes et al., 1995; Garrigues et al., 2015). One hypothesis to explain this apparent discrepancy is that the heterochromatin structuration controlled at the scale of the nucleosomal array by HPL-2 may help to define local boundaries with increased recombination occurring between such regions. Since H3K9me3 was largely unaffected in the *met-2(RNAi)* gonads, as previously observed (Bessler et al., 2010), our data suggest that MET-2-mediated H3K9me2 plays a chromatin structural role on its own, which might involve binding of other reader protein(s) in addition to HPL-2. Possible candidates could be malignant-brain-tumor (MBT)-domain-containing proteins, known to preferentially interact with H3K9me2, or chromatin-associated C2H2 zinc-finger proteins that modulate access to chromatin remodeling complexes (Koester-Eiserfunke and Fischle, 2011; Reddy and Villeneuve, 2004). Concerning the role of the MET-2-mediated compaction, we note that *met-2* deficiency increases the frequency of meiotic prophase chromosomal defects (Bessler et al., 2010). Thus, although MET-2 is not strictly essential for meiosis, it is required for faithful execution of the meiotic recombination program, and this may be linked to its involvement in nanoscale chromatin compaction.

(C) 2D FRET image of synapsed chromosomes in a wild-type nucleus (top), a *dpy-28(RNAi)*-depleted nucleus (middle), and a *kle-2(RNAi)*-depleted nucleus (bottom). Manual tracing of an individual chromosomes (dashed line) permits quantification of the FRET efficiencies (%) along the chromosome. Representative FRET (%) profiles are shown (right panels). For each condition, the line profile quantification was performed starting at the chromosome extremity marked by an asterisk. Scale bars, 1 μm.
See also Figure S6 and Table S1.

We also explored the structural roles of condensins, which are essential for chromosome condensation and the higher order threads of chromatin fibers (Houlard et al., 2015; Shintomi and Hirano, 2011). Besides their unique functions, condensin I and condensin II have also overlapping roles in the higher order structuration of chromosomes (Houlard et al., 2015; Nishide and Hirano, 2014). Mutations in condensin I subunits, including *dpy-28*, lead to an altered distribution and an increased crossover frequency at meiotic chromosomes (Mets and Meyer, 2009). These earlier observations are concordant with a reported increase and shift in the distribution of RAD-51 foci associated with double-strand break formation (Kleckner et al., 2004; Mets and Meyer, 2009) and may be explained by the change in the local structuration that we observed in vivo by FLIM-FRET.

Our technology reveals that condensin complexes are essential for the nanoscale compaction of chromatin as well. What could be the structural basis and role of this function? We find that condensins I and II both regulate the nanoscale compaction of heterochromatin, whereas condensin I knockdown affected the lowly compacted chromatin as well (Figure 7). The overlapping roles and functional divergence between the two types of complexes suggest that their binding may be different on pachytene chromosomes, similarly as in embryos, where condensins I and II are recruited partly to non-overlapping regions (Kranz et al., 2013).

The differential effects of condensins on chromatin compaction may explain topologically the recent finding in mice that condensin II confers the longitudinal rigidity to mouse meiotic chromosomes, whereas condensin I drives chromosome formation (Cuylen et al., 2011; Houlard et al., 2015). In this regard, we find that, along individual meiotic chromosomes, high-FRET condensed regions that potentially correspond to meiotic chromosomal axes are affected upon condensin II depletion. In contrast, intermediate-FRET regions, which may represent less compacted DNA loops protruding from the chromosome axes, are mostly perturbed upon condensin I knockdown (Figure 6C). It remains to be determined how the compaction regulated by HPL-2 and MET-2 links in with that controlled by condensins. Possibly, the high-FRET regions that persisted after condensin I knockdown are controlled by HPL-2/MET-2, particularly at the arms of the meiotic chromosomes where there is preferential HPL-2/MET-2 binding (Garrigues et al., 2015).

The observed differential compaction activities of condensin complexes may drive distinct morphological changes in the loop arrays along the chromosome axis, as manifested by the position of loops along DNA, the number of chromatin loops and the loop-size formation (Goloborodko et al., 2016; Kleckner et al., 2004; Mets and Meyer, 2009; Strick et al., 2004) (Figure 7). Moreover, our study highlights that events occurring at a smaller scale (controlled by HPL-2 and MET-2) and events at a larger scale (condensin dependent) are both required to achieve specific compaction states at chromosomal domains. The latter finding raises the question of how higher order looping and local nanoscale organization of chromosomes could be linked, as well as the question about the role of differential chromatin compaction states in meiotic cells.

In conclusion, we transferred the principle of FLIM-FRET to microscopic imaging in living animals that stably expressed fluorescent-tagged histones and demonstrate that this technology achieves non-invasive quantification and mapping of chromatin compaction states with high sensitivity and precision. Since this in vivo assay relies on collecting enough GFP-emitted photons to be able to extract representative and robust fluorescence lifetime values, a potential hurdle is the need to achieve stable, cell-type-appropriate, and sufficiently high expression of donor fluorophores. A limited level of expression may affect the recorded lifetime values and limit the range of detection of subtle changes in chromatin compaction. Furthermore, it is important to have experimental tissues that are readily accessible for microscopy. Although we succeeded to perform FRET measurements on germ cells within intact living worms, we noticed that, by dissecting gonads, we eliminated some out-of-focus fluorescence and obtained sharper FRET images. We expect that, at least in *C. elegans*, the dissection step could be avoided in case the expression of fluorescent-tagged histones is driven by somatic promoters. Despite these general requirements, the methodology should be readily transferrable to other model species. In mammals, it could be particularly interesting for early embryogenesis or hematopoietic studies. As emphasized by our functional studies on the HPL-2, MET-2, and condensin complexes, the technology also offers the prospect of performing in vivo RNAi library screens of candidate factors. In conclusion, our experimental system lays the basis for monitoring chromatin compaction in living organisms and offers the exciting prospect to explore the effects of genetic and environmental factors on chromatin compaction.

EXPERIMENTAL PROCEDURES

Worm Strains and Culture Conditions

Strains "GFP-H2B" and "2FPs-H2B" used in this study refer to the *C. elegans* strains EG4601 and EG6787, which have the following genotypes, respectively (further information is available on http://www.wormbase.org):

- EG4601: *oxIs279 [pie-1p::GFP::H2B + unc-119(+)]*; and
- EG6787: *oxSi487 [mex-5p::mCherry::H2B::tbb-2:3′UTR::gpd-2 operon::GFP::H2B::cye-1 3′UTR + unc-119(+)] II; unc-119(ed3) III.*

C. elegans strain N2 Bristol and strains "GFP-H2B" and "2FPs-H2B" were cultured at 20°C on nematode growth medium (NGM) agar plates seeded with *E. coli* strain OP50, following standard procedures (Brenner, 1974).

Worm Live-Imaging Preparation

For FRAP and FLIM-FRET acquisitions (discussed later), individually picked worms were put onto an unseeded NGM plate to wash off bacteria and were transferred onto a glass slide in a 10-μL drop of egg buffer (118 mM NaCl, 48 mM KCl, 2 mM $CaCl_2$*$2H_2O$, 2 mM $MgCl_2$*$6H_2O$, 25 mM HEPES [pH 7.3]). Worm gonads were dissected with a 23G syringe and immediately covered with a coverslip, sealed subsequently with nail varnish.

FLIM-FRET Acquisitions

FLIM-FRET experiments were carried out on strains GFP-H2B (donor alone: GFP-H2B protein) and 2FPs-H2B (donor and acceptor: GFP-H2B and mCherry-H2B). FLIM was performed using an inverted laser scanning multiphoton LSM780 microscope (Zeiss) equipped with an environmental black-walled chamber. Measurements were performed at 20°C with a 40× oil immersion lens, NA 1.3 Plan-Apochromat objective, from Zeiss. Two-photon excitation was achieved using a tunable Chameleon Ultra II (680–1,080 nm) laser (Coherent) to pump a mode-locked, frequency-doubled Ti:sapphire laser that provided sub-150-fs pulses at an 80-MHz repetition rate, with an output

power of 3.3 W at the peak of the tuning curve (800 nm). Enhanced detection of the emitted photons was achieved through the use of an HPM-100 module (Hamamatsu R10467-40 GaAsP hybrid photomultiplier tube [PMT]). The fluorescence lifetime imaging capability was provided by time-correlated single-photon counting (TCSPC) electronics (SPC-830; Becker & Hickl). TCSPC measures the time elapsed between laser pulses and the fluorescence photons.

GFP and mCherry fluorophores were used as a FRET pair. The optimal two-photon excitation wavelength to excite the donor (GFP) was determined to be 890 nm (Lleres et al., 2007). Laser power was adjusted to give a mean photon count rate of about 4.10^4–10^5 photons per second. For FLIM acquisition in *C. elegans* gonads, fluorescence lifetime measurements were acquired over 60 s, and fluorescence lifetimes were calculated for all pixels in the field of view (256 × 256 pixels). Particular regions of interest (e.g., full gonad or pachytene nuclei) were selected using SPCImage software (Becker & Hickl).

FLIM-FRET Analysis

FLIM measurements were analyzed using SPCImage software (Becker & Hickl). FRET results from direct interactions between donor and acceptor molecules (Förster, 1949). FRET reactions cause a decrease in the fluorescence lifetime of the donor molecules (GFP). The FRET efficiency (i.e., coupling efficiency) is calculated by comparing the FLIM values obtained for the GFP donor fluorophore in the presence and absence of the mCherry acceptor fluorophore. Mean FRET efficiency images were calculated as the FRET efficiency, $E\ FRET = 1 - (\tau DA/\tau D)$, where τ_{DA} is the mean fluorescence lifetime of the donor (GFP-H2B) in the presence of the acceptor (mCherry-H2B) expressed in 2FPs-H2B *C. elegans*, and τ_D is the mean fluorescence lifetime of the donor (GFP-H2B) expressed in GFP-H2B *C. elegans* in the absence of the acceptor. In the non-FRET conditions, the mean fluorescence lifetime value of the donor was calculated from a mean of the τ_D by applying a mono-exponential decay model to fit the fluorescence lifetime decays.

In the FRET conditions used, we applied a bi-exponential fluorescence decay model to fit the experimental decay curves $f(t) = a\,DA\ e^{-t/\tau DA} + b\,D\ e^{-t/\tau D}$. By fixing the non-interacting proteins' lifetime τ_D using data from control experiments (GFP-H2B *C. elegans* samples), the value of τ_{DA} was estimated. Then, the FRET efficiency, indicated here as *E FRET*, was derived by applying the following equation: $E\ FRET = 1 - (\tau DA/\tau D)$ at each pixel in a selected region of interest (ROI) using SPCImage software. ROIs represent pachytene nuclei in this study. The FRET distribution curves from these ROIs were displayed from the extracted associated matrix using SPCImage and then normalized and graphically represented using Excel and GraphPad Prism software. For each experiment, FLIM was performed on multiple pachytene cells from several independent dissected gonads (see figure legends and Table S1).

SUPPLEMENTAL INFORMATION

Supplemental Information includes Supplemental Experimental Procedures, six figures, and one table and can be found with this article online at http://dx.doi.org/10.1016/j.celrep.2017.01.043.

AUTHOR CONTRIBUTIONS

Conceptualization, D.L. and A.P.B.; Methodology, D.L.; Investigation, D.L., A.P.B., D.G.N., and A.P.; Formal Analysis, D.L. and D.G.N.; Data Curation, D.L.; Writing – Original Draft, D.L. and R.F.; Writing – Review & Editing, D.L., R.F., A.P.B., D.G.N., and D.P.X.; Funding Acquisition, D.L., R.F., D.P.X., and A.P.B.; Project Administration, R.F. and D.P.X.; Supervision, D.L. and R.F.

ACKNOWLEDGMENTS

We thank the members of our laboratories for helpful discussion and suggestions, M. Girardot for help with R statistical analysis, the Montpellier Rio Imaging Microscopy Facility for technical assistance, and the Caenorhabditis Genetics Center for strains. D.L. was supported by a Cancéropole GSO-Emergence grant (2014-E17). R.F. acknowledges grant support from the Fondation Recherche Médicale (FRM; grant DEQ20150331703) and the Agence Nationale de Recherche (ANR; grant "IMPRINT-RNA"). A.P.B. is supported by the Agence Nationale de la Recherche (ANR; grant "CeLeNeD"), the FRM (grant SPF20120523917), and INSERM.

Received: September 26, 2016
Revised: December 21, 2016
Accepted: January 19, 2017
Published: February 14, 2017

REFERENCES

Andersen, E.C., and Horvitz, H.R. (2007). Two C. elegans histone methyltransferases repress lin-3 EGF transcription to inhibit vulval development. Development *134*, 2991–2999.

Barnes, T.M., Kohara, Y., Coulson, A., and Hekimi, S. (1995). Meiotic recombination, noncoding DNA and genomic organization in Caenorhabditis elegans. Genetics *141*, 159–179.

Bessler, J.B., Andersen, E.C., and Villeneuve, A.M. (2010). Differential localization and independent acquisition of the H3K9me2 and H3K9me3 chromatin modifications in the Caenorhabditis elegans adult germ line. PLoS Genet. *6*, e1000830.

Bickmore, W.A. (2013). The spatial organization of the human genome. Annu. Rev. Genomics Hum. Genet. *14*, 67–84.

Boettiger, A.N., Bintu, B., Moffitt, J.R., Wang, S., Beliveau, B.J., Fudenberg, G., Imakaev, M., Mirny, L.A., Wu, C.T., and Zhuang, X. (2016). Super-resolution imaging reveals distinct chromatin folding for different epigenetic states. Nature *529*, 418–422.

Brenner, S. (1974). The genetics of Caenorhabditis elegans. Genetics *77*, 71–94.

Couteau, F., Guerry, F., Muller, F., and Palladino, F. (2002). A heterochromatin protein 1 homologue in Caenorhabditis elegans acts in germline and vulval development. EMBO Rep. *3*, 235–241.

Cremer, T., Küpper, K., Dietzel, S., and Fakan, S. (2004). Higher order chromatin architecture in the cell nucleus: on the way from structure to function. Biol. Cell *96*, 555–567.

Cremer, M., Grasser, F., Lanctôt, C., Müller, S., Neusser, M., Zinner, R., Solovei, I., and Cremer, T. (2008). Multicolor 3D fluorescence in situ hybridization for imaging interphase chromosomes. Methods Mol. Biol. *463*, 205–239.

Csankovszki, G., Collette, K., Spahl, K., Carey, J., Snyder, M., Petty, E., Patel, U., Tabuchi, T., Liu, H., McLeod, I., et al. (2009). Three distinct condensin complexes control C. elegans chromosome dynamics. Curr. Biol. *19*, 9–19.

Cuylen, S., Metz, J., and Haering, C.H. (2011). Condensin structures chromosomal DNA through topological links. Nat. Struct. Mol. Biol. *18*, 894–901.

Danzer, J.R., and Wallrath, L.L. (2004). Mechanisms of HP1-mediated gene silencing in Drosophila. Development *131*, 3571–3580.

Dixon, J.R., Selvaraj, S., Yue, F., Kim, A., Li, Y., Shen, Y., Hu, M., Liu, J.S., and Ren, B. (2012). Topological domains in mammalian genomes identified by analysis of chromatin interactions. Nature *485*, 376–380.

Förster, T. (1949). Experimental and theoretical investigation of the intermolecular transfer of electronic excitation energy. Z. Naturforsch. A *4*, 321–327.

Frøkjær-Jensen, C., Davis, M.W., Ailion, M., and Jorgensen, E.M. (2012). Improved Mos1-mediated transgenesis in C. elegans. Nat. Methods *9*, 117–118.

Garrigues, J.M., Sidoli, S., Garcia, B.A., and Strome, S. (2015). Defining heterochromatin in C. elegans through genome-wide analysis of the heterochromatin protein 1 homolog HPL-2. Genome Res. *25*, 76–88.

Gibcus, J.H., and Dekker, J. (2013). The hierarchy of the 3D genome. Mol. Cell *49*, 773–782.

Goloborodko, A., Marko, J.F., and Mirny, L.A. (2016). Chromosome compaction by active loop extrusion. Biophys. J. *110*, 2162–2168.

Hirano, T. (2005). Condensins: organizing and segregating the genome. Curr. Biol. *15*, R265–R275.

Houlard, M., Godwin, J., Metson, J., Lee, J., Hirano, T., and Nasmyth, K. (2015). Condensin confers the longitudinal rigidity of chromosomes. Nat. Cell Biol. *17*, 771–781.

Jenuwein, T., and Allis, C.D. (2001). Translating the histone code. Science *293*, 1074–1080.

Kelly, W.G., Xu, S., Montgomery, M.K., and Fire, A. (1997). Distinct requirements for somatic and germline expression of a generally expressed Caenorhabditis elegans gene. Genetics *146*, 227–238.

Kelly, W.G., Schaner, C.E., Dernburg, A.F., Lee, M.H., Kim, S.K., Villeneuve, A.M., and Reinke, V. (2002). X-chromosome silencing in the germline of C. elegans. Development *129*, 479–492.

Kleckner, N., Zickler, D., Jones, G.H., Dekker, J., Padmore, R., Henle, J., and Hutchinson, J. (2004). A mechanical basis for chromosome function. Proc. Natl. Acad. Sci. USA *101*, 12592–12597.

Koester-Eiserfunke, N., and Fischle, W. (2011). H3K9me2/3 binding of the MBT domain protein LIN-61 is essential for Caenorhabditis elegans vulva development. PLoS Genet. *7*, e1002017.

Kramer, J.M., French, R.P., Park, E.C., and Johnson, J.J. (1990). The Caenorhabditis elegans rol-6 gene, which interacts with the sqt-1 collagen gene to determine organismal morphology, encodes a collagen. Mol. Cell. Biol. *10*, 2081–2089.

Kranz, A.L., Jiao, C.Y., Winterkorn, L.H., Albritton, S.E., Kramer, M., and Ercan, S. (2013). Genome-wide analysis of condensin binding in Caenorhabditis elegans. Genome Biol. *14*, R112.

Lieberman-Aiden, E., van Berkum, N.L., Williams, L., Imakaev, M., Ragoczy, T., Telling, A., Amit, I., Lajoie, B.R., Sabo, P.J., Dorschner, M.O., et al. (2009). Comprehensive mapping of long-range interactions reveals folding principles of the human genome. Science *326*, 289–293.

Linhoff, M.W., Garg, S.K., and Mandel, G. (2015). A high-resolution imaging approach to investigate chromatin architecture in complex tissues. Cell *163*, 246–255.

Lleres, D., Swift, S., and Lamond, A.I. (2007). Detecting protein-protein interactions in vivo with FRET using multiphoton fluorescence lifetime imaging microscopy (FLIM). Curr. Protoc. Cytom. *Chapter 12*, Unit 12.10, 12.10.1–12.10-19.

Llères, D., James, J., Swift, S., Norman, D.G., and Lamond, A.I. (2009). Quantitative analysis of chromatin compaction in living cells using FLIM-FRET. J. Cell Biol. *187*, 481–496.

Luger, K., and Hansen, J.C. (2005). Nucleosome and chromatin fiber dynamics. Curr. Opin. Struct. Biol. *15*, 188–196.

Luger, K., Mäder, A.W., Richmond, R.K., Sargent, D.F., and Richmond, T.J. (1997). Crystal structure of the nucleosome core particle at 2.8 A resolution. Nature *389*, 251–260.

Lui, D.Y., and Colaiácovo, M.P. (2013). Meiotic development in Caenorhabditis elegans. Adv. Exp. Med. Biol. *757*, 133–170.

Maddox, P.S., Portier, N., Desai, A., and Oegema, K. (2006). Molecular analysis of mitotic chromosome condensation using a quantitative time-resolved fluorescence microscopy assay. Proc. Natl. Acad. Sci. USA *103*, 15097–15102.

Mets, D.G., and Meyer, B.J. (2009). Condensins regulate meiotic DNA break distribution, thus crossover frequency, by controlling chromosome structure. Cell *139*, 73–86.

Mora-Bermúdez, F., and Ellenberg, J. (2007). Measuring structural dynamics of chromosomes in living cells by fluorescence microscopy. Methods *41*, 158–167.

Nishide, K., and Hirano, T. (2014). Overlapping and non-overlapping functions of condensins I and II in neural stem cell divisions. PLoS Genet. *10*, e1004847.

Phillips-Cremins, J.E., Sauria, M.E., Sanyal, A., Gerasimova, T.I., Lajoie, B.R., Bell, J.S., Ong, C.T., Hookway, T.A., Guo, C., Sun, Y., et al. (2013). Architectural protein subclasses shape 3D organization of genomes during lineage commitment. Cell *153*, 1281–1295.

Reddy, K.C., and Villeneuve, A.M. (2004). C. elegans HIM-17 links chromatin modification and competence for initiation of meiotic recombination. Cell *118*, 439–452.

Richards, E.J., and Elgin, S.C. (2002). Epigenetic codes for heterochromatin formation and silencing: rounding up the usual suspects. Cell *108*, 489–500.

Sexton, T., Schober, H., Fraser, P., and Gasser, S.M. (2007). Gene regulation through nuclear organization. Nat. Struct. Mol. Biol. *14*, 1049–1055.

Shintomi, K., and Hirano, T. (2011). The relative ratio of condensin I to II determines chromosome shapes. Genes Dev. *25*, 1464–1469.

Stinchcomb, D.T., Shaw, J.E., Carr, S.H., and Hirsh, D. (1985). Extrachromosomal DNA transformation of Caenorhabditis elegans. Mol. Cell. Biol. *5*, 3484–3496.

Strick, T.R., Kawaguchi, T., and Hirano, T. (2004). Real-time detection of single-molecule DNA compaction by condensin I. Curr. Biol. *14*, 874–880.

Strukov, Y.G., and Belmont, A.S. (2009). Mitotic chromosome structure: reproducibility of folding and symmetry between sister chromatids. Biophys. J. *96*, 1617–1628.

Towbin, B.D., Meister, P., Pike, B.L., and Gasser, S.M. (2010). Repetitive transgenes in C. elegans accumulate heterochromatic marks and are sequestered at the nuclear envelope in a copy-number- and lamin-dependent manner. Cold Spring Harb. Symp. Quant. Biol. *75*, 555–565.

Tsai, C.J., Mets, D.G., Albrecht, M.R., Nix, P., Chan, A., and Meyer, B.J. (2008). Meiotic crossover number and distribution are regulated by a dosage compensation protein that resembles a condensin subunit. Genes Dev. *22*, 194–211.

Wallrath, L.L., and Elgin, S.C. (1995). Position effect variegation in Drosophila is associated with an altered chromatin structure. Genes Dev. *9*, 1263–1277.

Woodcock, C.L., and Dimitrov, S. (2001). Higher-order structure of chromatin and chromosomes. Curr. Opin. Genet. Dev. *11*, 130–135.